Paspalum urvillei and Setaria parviflora, two grasses naturally adapted to extreme iron-rich environments

Talita Oliveira de Araujo, M.-P. Isaure, Ghaya Alchoubassi, Katarzyna Bierla, Joanna Szpunar, Nicolas Trcera, Sandrine Chay, Carine Alcon, Luzimar Campos da Silva, Catherine Curie, et al.

▶ **To cite this version:**

Talita Oliveira de Araujo, M.-P. Isaure, Ghaya Alchoubassi, Katarzyna Bierla, Joanna Szpunar, et al.. Paspalum urvillei and Setaria parviflora, two grasses naturally adapted to extreme iron-rich environments. Plant Physiology and Biochemistry, 2020, 151, pp.144-156. 10.1016/j.plaphy.2020.03.014 . hal-02518238

HAL Id: hal-02518238
https://hal.inrae.fr/hal-02518238

Submitted on 25 Aug 2020

HAL is a multi-disciplinary open access archive for the deposit and dissemination of scientific research documents, whether they are published or not. The documents may come from teaching and research institutions in France or abroad, or from public or private research centers.

L'archive ouverte pluridisciplinaire **HAL**, est destinée au dépôt et à la diffusion de documents scientifiques de niveau recherche, publiés ou non, émanant des établissements d'enseignement et de recherche français ou étrangers, des laboratoires publics ou privés.

Plant Physiology and Biochemistry 151 (2020) 144–156

Contents lists available at ScienceDirect

Plant Physiology and Biochemistry

journal homepage: www.elsevier.com/locate/plaphy

Research article

Paspalum urvillei and *Setaria parviflora*, two grasses naturally adapted to extreme iron-rich environments

Talita Oliveira de Araujo[a,d], Marie-Pierre Isaure[b], Ghaya Alchoubassi[b], Katarzyna Bierla[b], Joanna Szpunar[b], Nicolas Trcera[c], Sandrine Chay[d], Carine Alcon[d], Luzimar Campos da Silva[a], Catherine Curie[d], Stephane Mari[d,*]

[a] Universidade Federal de Viçosa, Laboratório de Anatomia Vegetal, Viçosa, 36570-900, Brazil
[b] Universite de Pau et des Pays de l'Adour, E2S UPPA, CNRS, IPREM UMR 5254, Hélioparc, 64053 Pau, France
[c] Synchrotron SOLEIL, l'Orme des Merisiers Saint Aubin BP48, 91192, Gif-sur-Yvette Cedex, France
[d] BPMP, Univ Montpellier, CNRS, INRAE, Institut Agro, Montpellier, France

ARTICLE INFO

Keywords:
Paspalum urvillei
Setaria parviflora
Setaria viridis
Oryza sativa
Perls-DAB method
μXRF
μXANES
Iron plaque
Vacuole
Chloroplast
Ferritin
Citrate
Malate

ABSTRACT

Paspalum urvillei and *Setaria parviflora* are two plant species naturally adapted to iron-rich environments such as around iron mines wastes. The aim of our work was to characterize how these two species cope with these extreme conditions by comparing them with related model species, *Oryza sativa* and *Setaria viridis,* that appeared to be much less tolerant to Fe excess. Both *Paspalum urvillei* and *Setaria parviflora* were able to limit the amount of Fe accumulated within roots and shoots, compared to the less tolerant species. Perls/DAB staining of Fe in root cross sections indicated that *Paspalum urvillei* and *Setaria parviflora* responded through the build-up of the iron plaque (IP), suggesting a role of this structure in the limitation of Fe uptake. Synchrotron μXRF analyses showed the presence of phosphorus, calcium, silicon and sulfur on IP of *Paspalum urvillei* roots and μXANES analyses identified Fe oxyhydroxide (ferrihydrite) as the main Fe form. Once within roots, high concentrations of Fe were localized in the cell walls and vacuoles of *Paspalum urvillei*, *Setaria parviflora* and *O. sativa* whereas *Setaria viridis* accumulated Fe in ferritins. The Fe forms translocated to the shoots of *Setaria parviflora* were identified as tri-iron complexes with citrate and malate. In leaves, all species accumulated Fe in the vacuoles of bundle sheath cells and as ferritin complexes in plastids. Taken together, our results strongly suggest that *Paspalum urvillei* and *Setaria parviflora* set up mechanisms of Fe exclusion in roots and shoots to limit the toxicity induced by Fe excess.

1. Introduction

Iron (Fe) is an essential micronutrient that is absorbed by roots of grasses as Fe^{3+}-phytosiderophores complexes and follows the transpiration stream to the shoot along with other nutrients and minerals (Nozoye et al., 2011). Despite being required in chloroplasts and mitochondria to be used as an enzymatic cofactor in a wide range of metabolic processes (Balk and Schaedler, 2014), when in excess, ferrous ions can promote the generation of reactive oxygen species and oxidative stress (Dinakar et al., 2010). Nevertheless, some species are naturally adapted to tolerate extremely high concentrations of metals in their environment, using two distinct strategies: some species will avoid the built up of metals in the organs, particularly in leaves, they are termed "excluders" whereas other species will promote the storage of metals in above-ground organs, these plants are known as "hyperaccumulators" (van der Ent et al., 2013). Hyperaccumulation of Ni, Zn, Cd, As, Cu, Co, Mn, Pb, Se, Tl and rare earth elements (REE) has been reported (van der Ent et al., 2013; Reeves et al., 2018). Iron hyperaccumulation has been much less reported, probably because Fe has a low bioavailability caused by the low solubility of iron oxyhydroxides in natural environments and instead, acts as a limiting factor for plant growth. Therefore the identification of true Fe hyperaccumulators is less clearly established than for other trace elements. Nevertheless, there are some studies reporting Fe tolerance and hyperaccumulation in *Imperata cylindrica* (grass family, Poacae) from the acidic mining area of the Tinto River banks in the Iberian Pyritic Belt in Spain (Rodriguez et al., 2005; de la Fuente et al., 2017). Contrary to hyperaccumulators, true "excluder" plants have received much less attention (Bothe and Slomka, 2017).

To deal with Fe excess, plants employ mechanisms such as induction of antioxidant system (Stein et al., 2014), reorganization of the photosynthetic apparatus (Pereira et al., 2014; Muller et al., 2015) and

* Corresponding author.
E-mail address: stephane.mari@inrae.fr (S. Mari).

https://doi.org/10.1016/j.plaphy.2020.03.014
Received 20 November 2019; Received in revised form 17 February 2020; Accepted 12 March 2020
Available online 18 March 2020
0981-9428/ © 2020 The Authors. Published by Elsevier Masson SAS. This is an open access article under the CC BY license (http://creativecommons.org/licenses/BY/4.0/).

detoxification and/or sequestration in sites where Fe will not cause damage to cell, *i.e.* vacuoles and apoplastic space (Briat et al., 2010a; Zhang et al., 2012). The presence of an iron plaque (IP) can be considered as a mechanism of resistance, since it is due to Fe precipitation on the root surface, avoiding the over-accumulation of iron in leaf tissues (Green and Etherington, 1977). The IP formation occurs in roots of wetland plant where Fe is spontaneously precipitated due to oxidizing microenvironments normally created around roots of aquatic plants (Xu et al., 2009). Thus, Fe^{2+} is oxidized into Fe^{3+}, which precipitates on the root surface, thereby creating a smooth regular reddish precipitate or irregular plaque coating on root surfaces (Pereira et al., 2014; Tripathi et al., 2014).

The adsorption of trace metals and nutrients is the most important characteristic of IP. A significant amount of metals bind to IP through the formation of complexes thanks to the high affinity of Fe hydroxide for different metals (Batty et al., 2000; Liu et al., 2011). Extensive efforts to understand the role of IP in metal sequestration and translocation have yielded contrasting results. Some authors agree that IP acts as a resistance barrier for metal(loids) translocation, and this barrier can function by either acting as an adsorbent of toxic elements or by simply being a physical obstacle (Pi et al., 2011; Huang et al., 2012). As an illustration, iron plaques have been demonstrated to sequester arsenic in the wetland plants *Typha latifolia* (Hansel et al., 2002; Blute et al., 2004), *Phragmites australis* (Pardo et al., 2016), *Phalaris arundinacea* (Hansel et al., 2002), and rice *Oryza sativa L* (Liu et al., 2006). Other metals such as Cu, Mn, Pb and Zn were also detected in IP from *Spartina alterniflora* (Feng et al., 2015; Xu et al., 2018) and *Phalaris arundinacea* (Hansel et al., 2001).

Alternatively, IP may act as a buffer and reservoir in nutrient uptake, particularly during the time of diminished supply of nutrients (Hu et al., 2007; Williams et al., 2014). In all cases, the nature of Fe phases in IP but also the plant species and the ionic species are likely involved in metals and metalloids uptake (Pereira et al., 2014; Batty et al., 2000; Hansel et al., 2001). Ferric iron is the predominant oxidation state of Fe on IP. Amorphous ferric oxyhydroxides, ferrihydrite, goethite (α-FeOOH), and lepidocrocite (γ-FeOOH) are commonly found as the main mineral phases in IP (Liu et al., 2006; Bacha and Hossner, 1977; Chen et al., 1980; Taylor et al., 1984; Stcyr et al., 1993). In highly acidic conditions, jarosite, a sulfur-rich mineral, accumulates in the IP of *Imperata cylindrical* (Rodriguez et al., 2005; Amils et al., 2007). Ferrous Fe too has been identified in IP of some species such as *Phragmites australis* (Wang and Peverly, 1996, 1999). In *Phalaris arundinacea* and *Typha latifolia,*Fe(II) was detected as siderite ($FeCO_3$) in addition to a mixture of ferryhydrite, goethite, lepidocrocite and ferric phosphate (Hansel et al., 2001, 2002).

Plants which develop IP on roots are able to better survive in contaminated soils (Taylor et al., 1984) by avoiding toxic buildup of metals in their aerial parts. To understand the role of IP in Fe absorption by the root, it is essential to have a clear description of the IP composition and of the Fe distribution strategy in roots. Chemical imaging techniques have become a key component of the toolbox to investigate metal distribution in plants. To localize Fe, histochemical staining using Perls-diaminobenzidine (DAB) has proved powerful to locate both Fe^{3+} and Fe^{2+} in plants at the cell level (Roschzttardtz et al., 2009). Since the method requires fixation and dehydration steps where loosely bound Fe species can be lost, it is useful to apply a complementary technique in which the sample preparation differs. In this context, micro X-ray fluorescence (μXRF) is of high interest due to its high sensitivity and the possibility to analyze hydrated frozen samples, which minimizes artifacts resulting from sample preparation (Sarret et al., 2013). Furthermore, μXRF can be combined with micro X-ray absorption near edge structure spectroscopy (μXANES) to probe the chemical form of metals in the same samples (Sarret et al., 2013; Salt et al., 2002; Isaure et al., 2015).

Inside the plant, Fe is translocated associated with suitable chelating molecules because of high reactivity and poor solubility (Kobayashi et al., 2012). Citrate was identified as the main Fe ligand in xylem sap of tomato plants (Rellan-Alvarez et al., 2010). Besides citrate, some studies have indicated malate and nicotianamine as organic molecules, which form a complex with iron (Takahashi et al., 2003; Grillet et al., 2014). Nothing is known about the long-distance Fe transport in Fe hyperaccumulator and hypertolerant plants, and therefore the identification, speciation and quantification of Fe transport forms in xylem sap are crucial to understand this long-distance transport. This knowledge is the basis to understand how the metal is transported across membranes and delivered to its final target.

The perennial grasses *Paspalum urvillei* Steudel and *Setaria parviflora*, native species from South America, were identified among the few species able to grow spontaneously at the margins of decantation ponds of an Fe ore pelletizing industry located in Brazil, in the Ubu district (municipality of Anchieta, state of Espìrito Santo, South-Eastern Brazil) (de Araujo et al., 2014). These ponds are supplied with water from the mining system and plumbing of the iron ore pelletizing industry, therefore creating an environment rich in iron particles. *Paspalum urvillei* and *Setaria parviflora* were further described as highly tolerant to Fe excess (de Araujo et al., 2014; Santana et al., 2014) and the formation of IP was observed around the roots (de Araujo et al., 2015).

In this study, by combining Perls/DAB histochemistry, μXRF, μXANES and chromatography coupled to mass spectrometry, we shed some light on the responses of *Paspalum urvillei* and *Setaria parviflora* to excess Fe and uncover new cellular Fe accumulation sites in response to excess.

2. Materials and methods

2.1. Growth conditions and treatment application

Seeds of *Paspalum urvillei* Steudel (Poaceae), *Setaria parviflora* and *Setaria viridis* were grown in a glasshouse (average temperature 23 °C), in plastic pots containing 0.5 L of quartz sand and 2.25 L of Humin substrate N2 Neuhaus (Klasmann-Deilmann, Bremen, Germany) irrigated with tap water for approximately 10 days. Plantlets with 3 leaves were quickly washed in tap water, rinsed and transferred to 2.4 L boxes containing Hoagland nutrient solution, at full ionic strength, with aeration every 4 h, at pH 5.0. After that, these plants were cultivated in growth chamber with 14 h light at 28 °C and 10 h dark at 25 °C, at 80% humidity, for one week in solution containing 0.5 mM $NH_4H_2PO_4$, 3 mM KNO_3, 2 mM $Ca(NO_3)_2{\cdot}4H_2O$, 1 mM $MgSO_4{\cdot}7H_2O$, 23.13 μM H_3BO_3, 4.57 μM, $MnCl_2{\cdot}4H_2O$, 0.382 μM $ZnSO_4\cdot7H_2O$, 0.16 μM, $CuSO_4{\cdot}5H_2O$ and 0.0695 μM MoO_3. Fe-sufficient plants were fed with 0.1 mM Fe(III)-citrate and Fe-excess plants were fed with 7 mM Fe(III)-citrate during 6 days. This solution was renewed every 3 days. Iron citrate stock solutions were prepared by mixing $FeCl_3$ with a 4-fold molar excess of citric acid and by adjusting the pH to 5.4 with KOH. For rice, seeds were germinated in water for 5 days and then transferred in hydroponic medium as described above.

2.2. Fe accumulation and localization by histochemical staining

To quantify the Fe concentration, plants (17 days old) were separated in leaves and roots. Roots were washed with dithionite–citrate–bicarbonate to eliminate the Fe aggregated at the root surface (Taylor and Crowder, 1983). Root and leaf samples (10–30 mg dry weight) were mineralized with a SpeedWave Two (Berghof Products, Eningen, Germany) in 1 ml of 48% HNO_3 and 7.5% H_2O_2, 3 min at 100 °C, 20 min at 180 °C, and 10 min at 140 °C. Fe concentration was determined by atomic emission spectroscopy with a Microwave Plasma Atomic Emission Spectroscope (MP-AES, Agilent), using manufacturer's standard solutions to establish calibration curves.

In order to determine the Fe location, fragments from different regions of leaf blades (basal, median and apical region) and root (meristematic, elongation and differentiation zone) were vacuum infiltrated

with fixation solution containing 2% (w/v) paraformaldehyde, 1% (v/v) glutaraldehyde, 1% (w/v) caffeine in 100 mM phosphate buffer (pH 7) for 30 min and incubated for 24 h in the same solution. The fixated fragments were washed with 0.1 M phosphate buffer (pH 7.4) three times, and dehydrated in successive baths of 50%, 70%, 90%, 95%, and 100% ethanol, butanol/ethanol 1:1 (v/v), and 100% butanol. Then, the fragments were embedded in the Technovit 7100 resin (Kulzer) according to the manufacturer's instructions and thin sections (5 μm thickness) were made. Histochemical Fe staining was realized by the Perls-DAB method to highlight total iron including both ferric and ferrous species (Roschzttardtz et al., 2009).

Fe staining images were captured using an Olympus BX-61 microscope (Olympus, Tokyo, Japan) equipped with Jenoptik ProgRes C5 digital camera (Jenoptik, Jena, Germany) in the PHIV (Histology and plant Cell imaging platform) imaging platform.

2.3. Elemental distribution by μXRF and Fe speciation by Fe K-edge μXANES

Fresh fragments from roots were immersed in a cryo-embedding Optimum Cutting Temperature compound (OCT, Sakura Finetek, Leiden, The Netherlands) and rapidly frozen in liquid nitrogen. They were kept at −80 °C until preparation of cryo-sections. The frozen blocks were then sectioned (25 μm thickness) in the transversal plane using a cryomicrotome just before measurements. The resulting cross-sections were deposited on Ultralene films (Spex Certiprep) and kept in liquid nitrogen until measurements.

Micro-XRF and μXANES measurements were performed on LUCIA beamline at the SOLEIL synchrotron (Saclay, France (Vantelon et al., 2016),). The X-ray beam was monochromatized with a Si(111) double-crystal monochromator, and focused using Kirkpatrick-Baez mirrors to a spot on the sample of 3 μm × 3 μm. Measurements were carried under vacuum and at −120 °C with a N_2 liquid cryostat to limit beam damage and minimize metal redistribution and speciation change.

For elemental mapping, μXRF was performed on iron plaques from root sections with an incident energy of 7300 eV, a step size of 3 μm and a dwell time of 1s/pixel. Elemental fluorescence signal was recorded using a four-element silicon drift diode (SDD) detector. The fluorescence signal was then deconvoluted from fluorescence background and elemental overlapping to obtain elemental maps. Then, Fe species were studied using Fe K-edge XANES on regions of interest selected from μXRF mapping, using the same lateral resolution and in fluorescence mode. Spectra were collected in the 7050–7250 eV range, with a sampling step of 2 eV between 7050 and 7100 eV, 0.2 eV from 7100.2 to 7160 eV, and 1 eV between 7161 and 7250 eV. Three or four XANES spectra were acquired on various positions distinct from a few microns, checked for similarity, and averaged to improve the signal-to-noise ratio. Data were calibrated with metallic Fe background subtracted and normalized using a linear or two-degree polynomial function with Athena software (Ravel and Newville, 2005). Fe XANES spectra were also collected on Fe(II) and Fe(III) reference compounds prepared as pressed pellets: hematite Fe_2O_3, ferrihydrite $5Fe_2O_3.9H_2O$, goethite (FeOOH), Fe(III)phosphate $Fe_3(PO_4).2H_2O$, chromite ($FeCr_2O_4$) and siderite ($FeCO_3$). Iron plaques spectra were compared to these reference spectra and to spectra that we have previously collected (Grillet et al., 2014). A fingerprint approach was then used to fit IP spectra with Fe reference compounds. The quality of the fits was evaluated by the normalized sum-squares residuals NSS ($NSS = \Sigma[\mu_{experimental} - \mu_{fit}]^2 / \Sigma[\mu_{exp}]^2 \times 100$) in the 7090–7225 eV range. The pre-edge structures were also examined by subtracting the pre-edge background modeled by an erf function taken a few eV before and after the pre-edge.

2.4. Analysis of metal complexes using HILIC-ICP-MS

Analytical reagent grade chemicals such as acetonitrile, acetic acid, formic acid, nitric acid and ammonia were purchased from Sigma-Aldrich. Ultrapure water (18MΩ.cm) was obtained from a Milli-Q system (Millipore, Guyancourt, France). The isotopically enriched ^{58}Fe (99.81% enrichment) was purchased from STB Isotope Germany GmbH (Hamburg, Germany).

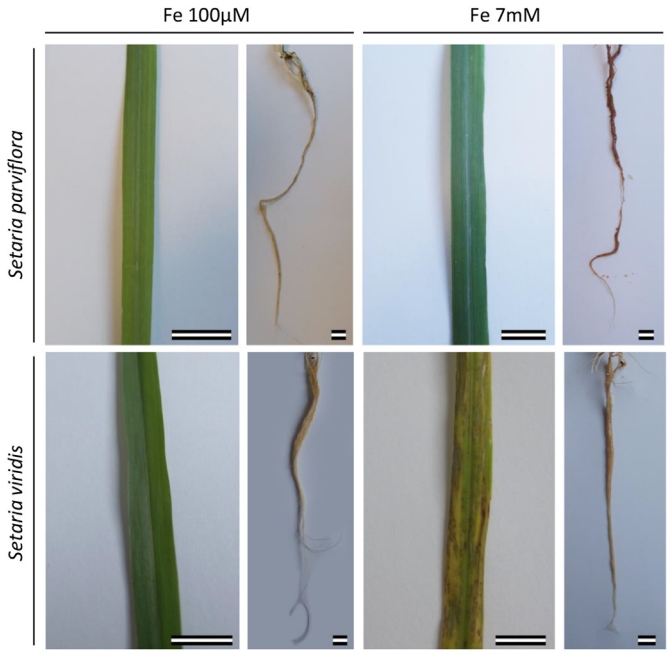

Fig. 1. Visual symptoms of Fe toxicity on *Setaria parviflora* and *Setaria viridis* plants. Ten day-old seedlings were grown for 6 days in medium supplemented with 0.1 mM or 7 mM Fe-citrate. Bar = 1 cm.

HILIC HPLC separations were performed using a 1200 HPLC system (Agilent, Tokyo, Japan). ICP-MS detection was achieved using a model 7700 instrument (Agilent) fitted with platinum cones, 1 mm i.d. injector torch. 7.5% of oxygen was added to plasma gas to avoid carbon deposit on the cones. The HILIC ICP MS coupling was done via Scott spray chamber cooled to −5 °C.

The column used for HILIC separation was a SeQuant®Zic®-cHILIC (150 × 2.1 mm, 3 μm 100 Å) column (Merck). Gradient elution, at a flow rate of 0.2 ml min^{-1}, was carried out using eluent A (acetonitrile), and eluent B (25 mM ammonium acetate pH 5.5). The gradient program was: 0–1min 5% B, 1–10 min up to 20% B, 10–13.5 min 20% B, 13.5–17 min up to 40% B, 17–21 min 40% B, 21–21.01 min down to 5% B, 21.01–30 min 5% B. Samples were diluted with ammonium acetate, divided in aliquots of 10 μL to which standard of ^{58}Fe was added in order to create calibration curve. Later on acetonitrile was added to obtain a 1:2, sample to acetonitrile ratio, vortexed and centrifuged. A 2 μL aliquot of the supernatant was injected into the HILIC column each time. The chromatographic conditions were optimized in order to ensure the best separation of the compounds, maximum recovery from the column and optimal ionisation conditions for electrospray ionisation. Additionally, the use of this separation technique requires very limited sample preparation, which helps with preservation of Fe complexes that are extremely prone to dissociation.

2.5. Analysis for metal complexes using HILIC-ESI-MS

For HILIC-ESI-MS the HPLC system Ultimate 3000 UPLC pump (Dionex, Paris, France) was connected to an LTQ Orbitrap Velos mass spectrometer (Thermo Fisher Scientific, Bremen, Germany). The coupling was achieved via a heated electrospray ionisation source (H-ESI II) (Thermo Fisher Scientific) or Orbitrap Q Exactive Plus. The chromatographic separation conditions were as given in the previous paragraph. The ion source was operated in the positive at 3.0 kV. The vaporizer temperature of the source was set to 250 °C and the capillary

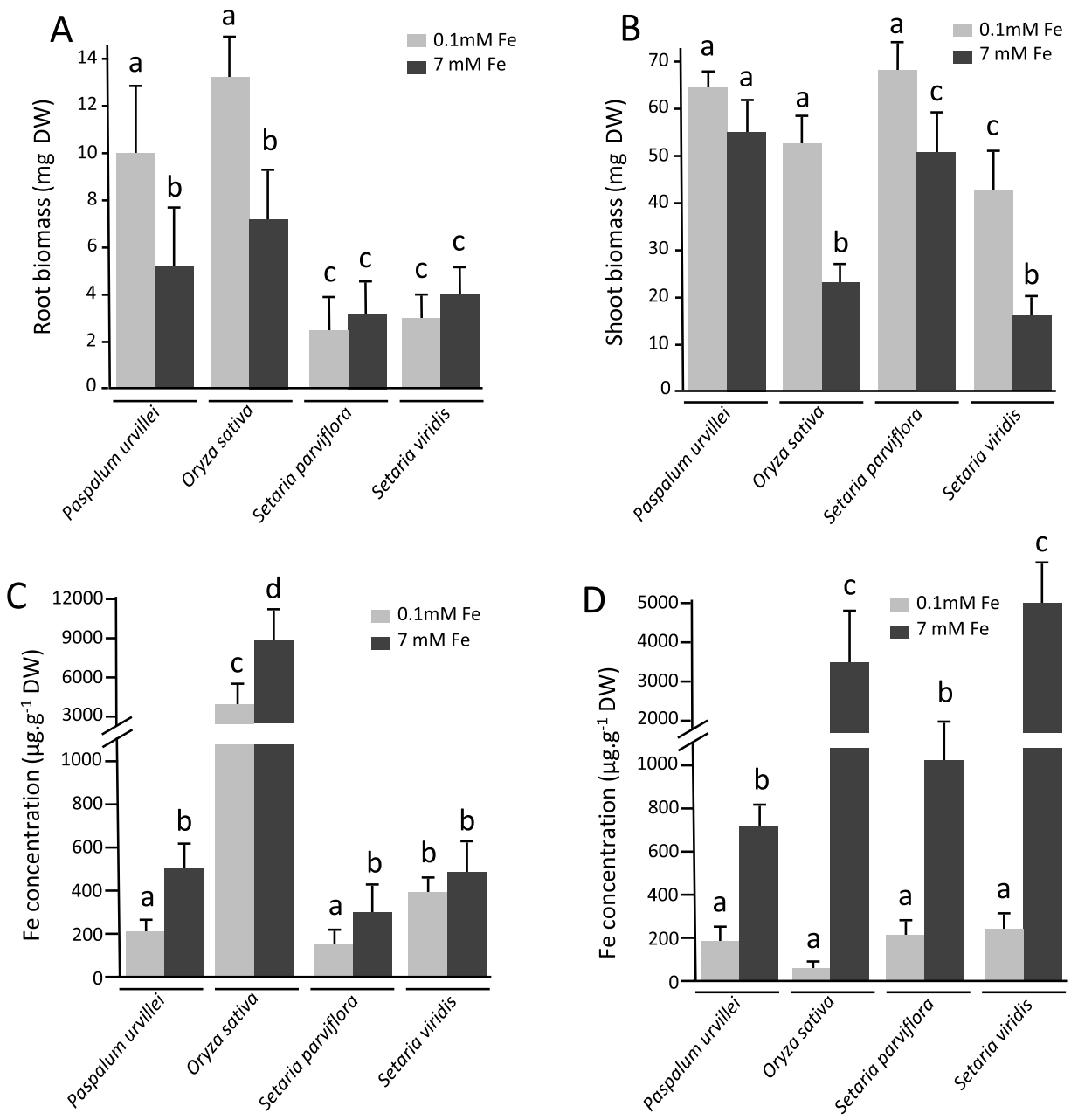

Fig. 2. Biomass and Fe concentration of roots and shoots of *Paspalum urvillei*, *Oryza sativa*, *Setaria parviflora* and *Setaria viridis* plants grown in standard and excess Fe. 10 day-old seedlings were grown for 6 days in medium supplemented with 0.1 mM or 7 mM Fe-citrate. (A) root biomass, (B) shoot biomass, (C) Fe concentration on roots, (D) Fe concentration in shoots. Values are average ± SD, values followed by the same letter do not differ by Tukey's test at 5% probability.

temperature to 350 °C. In full MS mode, the resolution was set at 100 000 or 280 000 (FWHM at m/z 400).

2.6. Statistical analysis

The experimental design adopted was randomized with four repetitions and five or two treatments. Data were subjected to analysis of variance (ANOVA), and means were compared by Tukey test at 5% probability, using statistical software SAEG 9.0 UFV.

3. Results

3.1. Analysis of Fe tolerance and accumulation

Paspalum urvillei and *Setaria parviflora* have been described as being tolerant to Fe excess (de Araujo et al., 2014). To further confirm the Fe tolerant behavior of these two species, we compared the tolerance to high concentrations of Fe-citrate of *Paspalum urvillei* and *Setaria parviflora* young plants with, respectively, rice (*Oryza sativa* cv nipponbare) and *Setaria viridis*, two model species used here as reference. The visual symptoms of standard and excess Fe on *Setaria parviflora* and *Setaria viridis* are illustrated in Fig. 1. Exposure to high Fe provoked the formation of brow necrotic spots in *Setaria viridis* leaves, whereas leaves from *Setaria parviflora* did not show any visible sign of toxicity. Similar symptoms were observed when comparing *Paspalum urvillei* and *Oryza sativa* (data not shown). Roots of *Setaria parviflora* displayed an intense brown coloration in Fe excess corresponding to the formation of the iron plaque and this phenomenon was almost absent in *Setaria viridis* (Fig. 1). The shoot biomass of *Paspalum urvillei* and *Setaria parviflora* plants was not significantly affected by an exposure to 7 mM Fe, compared to control media, whereas Fe excess provoked a two-fold reduction in biomass for *Oryza sativa* and *Setaria viridis* (Fig. 2A). This

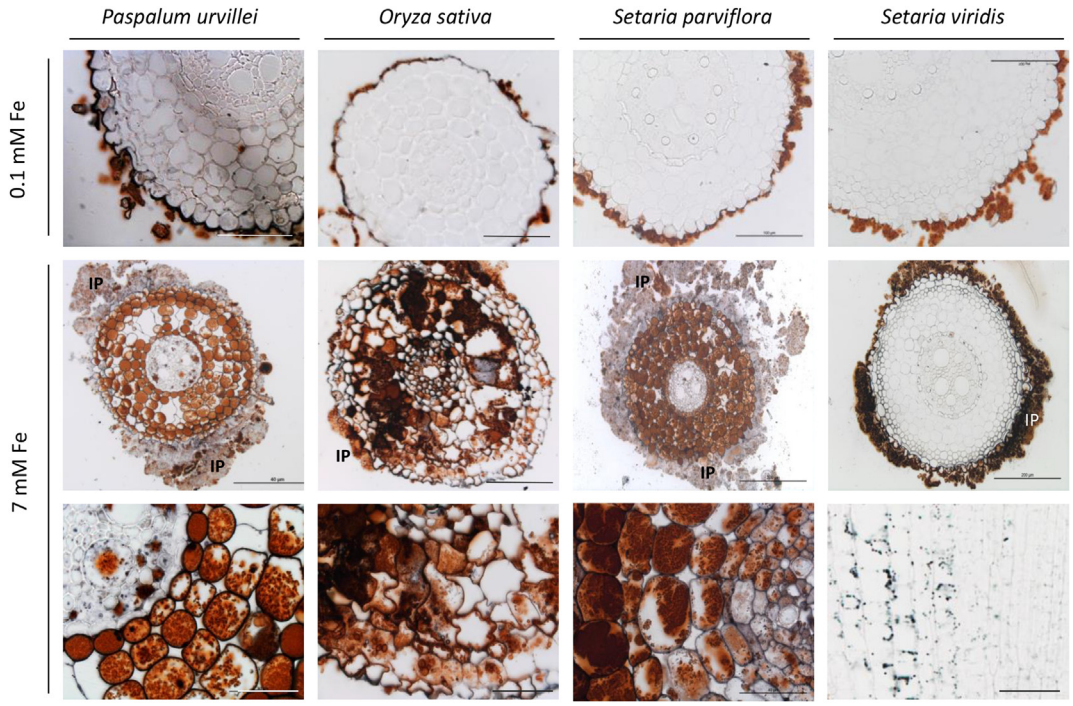

Fig. 3. Fe localization in root sections of *P. urvillei*, *O. sativa*, *S. parviflora* and *S. viridis*. Plants were treated with 0.1 mM or 7 mM Fe-Citrate during 6 days and root samples were further fixed and embedded in resin. Sections were submitted to Perls/DAB staining. IP, Iron plaque. Bar = 200 μm unless stated otherwise.

result further confirmed the Fe tolerance capacity of *Paspalum urvillei* and *Setaria parviflora*. In roots, Fe excess induced a reduction of growth that was equivalent for *P. urvillei* and *O. sativa*, whereas the root biomass of both *Setaria* species was not significantly affected by the Fe treatments (Fig. 2B).

Having established that *Paspalum urvillei* and *Setaria parviflora* are well-suited species to study responses to Fe excess, we then measured the Fe content in roots and shoots of plants grown on the two Fe regimes. In control condition (0.1 mM Fe-citrate) no significant difference in Fe concentration was observed in leaves of the four species (Fig. 1C). Iron excess had a moderate effect on the shoot Fe concentration of *Paspalum urvillei* and *Setaria parviflora* with a 3–4 fold increase in Fe accumulation whereas *Oryza sativa* and *Setaria viridis* shoots accumulated massive amounts of Fe, representing *ca* 50-fold increase, relative to standard Fe treatment (Fig. 2C). The exposure to Fe excess induced a limited increase in Fe accumulation in roots of *Paspalum urvillei*, *Setaria parviflora* and *Setaria viridis* whereas roots of *O. sativa* overaccumulated Fe, reaching up to 9000 ppm in response to Fe excess (Fig. 2D). From these results, we concluded that both *Paspalum urvillei* and *Setaria parviflora* plants were able to tolerate high concentrations of Fe in the medium with a very moderate effect in growth that could be attributed to their capacity to restrict Fe accumulation in their organs, when compared to the less tolerant species *Oryza sativa* and *Setaria viridis*.

To gain further insights in the tolerance mechanisms set up by *Paspalum urvillei* and *Setaria parviflora*, we studied Fe localization in roots and shoots in control and excess conditions. In standard condition, for all species, Fe was only visible as aggregates around the roots, corresponding to the iron plaque (IP) (Fig. 3). Upon exposure to 7 mM Fe-citrate, roots of the four species displayed different behavior. *Paspalum urvillei* and *Setaria parviflora* roots had built up a significant iron plaque, compared to *Oryza sativa* and *Setaria viridis* (Fig. 3, middle row). Within the root tissues of *Paspalum urvillei* and *Setaria parviflora*, Fe deposits completely filled the entire volume of all cortex cells. Additionally, a strong staining was visible around the epidermal and cortical cells and this staining was attributed to the cell walls. The strong difference in Fe accumulation between epidermal-cortical cells and the central cylinder indicated that the endodermis was playing a central role in the control of Fe loading into the vascular system. To a lesser extent, rice roots also accumulated high concentrations of Fe inside cells. Strikingly, the iron staining in the central cylinder was as intense as in the cortex, suggesting that, contrarily to *Paspalum urvillei* and *Setaria parviflora*, the endodermis was not such a barrier for the movement of Fe towards the conductive elements of the stele. Finally, root cells of *Setaria viridis* did not accumulate Fe in the vacuoles as the other species, instead, Fe-rich dot-shaped deposits were visible within cells. These Fe-rich structures were identical to Fe-ferritin complexes previously described in both roots and leaves of *Arabidopsis thaliana* plants treated with iron excess (Roschzttardtz et al., 2009; Bournier et al., 2013).

3.2. Metals distribution and speciation analyses in the iron plaque by μXRF and Fe K-edge μXANES

Micro-XRF and Fe K-edge μXANES were carried out in IP and roots of *Paspalum urvillei* to map the distribution of Fe and other elements and determine the Fe chemical species, respectively.

Elemental maps of roots exposed to 0.1 mM Fe-citrate showed that Fe was distributed as a thin layer deposited at the surface of epidermal cells. After saturating the Fe signal to pinpoint potential lower Fe concentrations, maps showed that the metal was strictly localized in the epidermis as a thick layer but neither in cortex nor endodermis (Fig. 4A "Fe sat"). In addition to Fe, phosphorus, calcium, silicon and manganese were visualized near the epidermis as observed on the bicolor and tricolor maps (Fig. 4A). In contrast, potassium and sulfur were located within the epidermis, cortex, and vascular system but were not highly concentrated in IP.

In roots exposed to Fe excess, the layer of IP was thicker (25 μm at 7 mM Fe versus 10 μm at 0.1 mM Fe) and contained a higher amount of Fe as attested by the change in Fe scale (Fig. 4B). Interestingly, in signal saturation conditions, we observed that Fe was strictly located in IP for the low exposure while Fe entered the root and cortex cells, and was finally retained in endodermis for the excess condition (Fig. 4B "Fe sat"). These results are in agreement with the histochemical staining shown above (Fig. 3). The amount of Ca also increased in IP while other

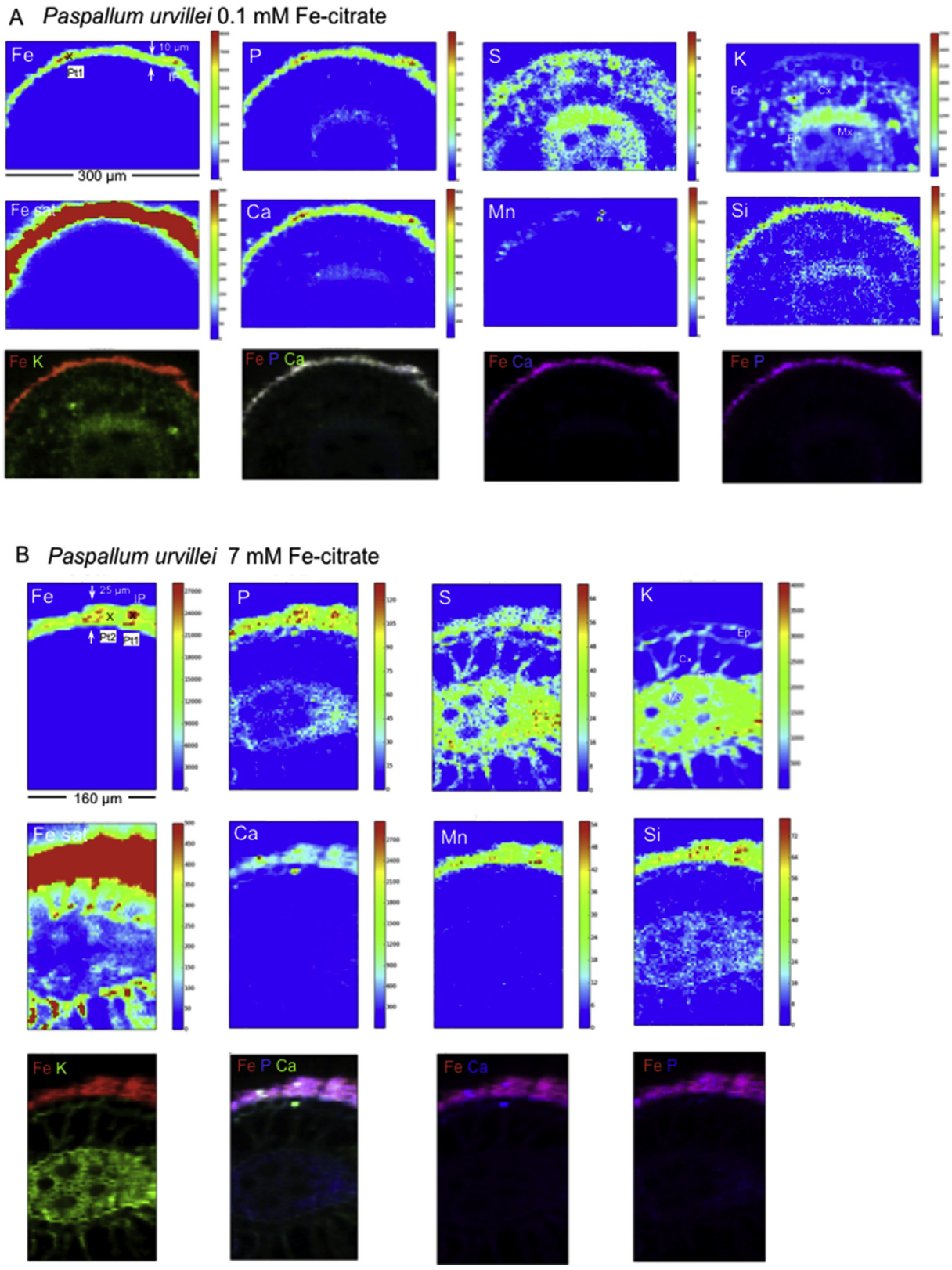

Fig. 4. Elemental distribution (µXRF) on *Paspalum urvillei* roots. **A, B:** Cryo cross-sections of plants treated with 0.1 mM (A) and 7 mM Fe-Citrate (B) respectively, during 6 days and elemental distribution of iron, phosphorus, sulfur, potassium, iron saturation, calcium, manganese, and silicon. Tricolor and bicolor maps were also shown to highlight co-location (lower line in A and B). Energy = 7.3 keV, step size = 3 µm, counting rate = 1s/pixel. The crosses annotated "Pt" indicate the areas where µXANES spectra were collected in these maps. The color bars indicate fluorescence intensity. Ep = epidermis; Cx = cortex; En = endodermis; Mx = metaxylem, IP = iron plaque. (For interpretation of the references to color in this figure legend, the reader is referred to the Web version of this article.)

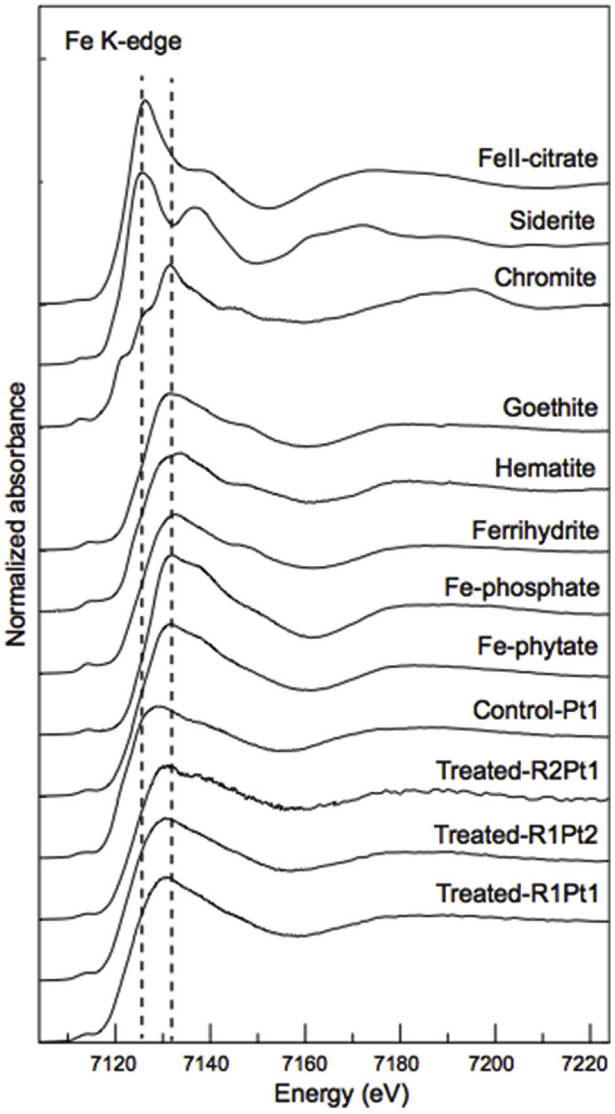

Fig. 5. Fe K-edge μXANES spectra collected on iron plaque of *Paspalum urvillei* treated with 0.1 mM (Control) and 7 mM (Treated) Fe-citrate compared to Fe reference spectra. Dotted lines indicate the shift between Fe(II)reference spectra and Fe(III) reference spectra.

elements remained unchanged. Co-localization of Fe with phosphorus, calcium, silicon and sulfur, indicated the presence of these elements in IP (Fig. 4).

Some biological preparations, particularly using chemical fixation and resin, can alter cellular materials and the location of key associated elements. Synchrotron μX-ray fluorescence requires no sample pre-treatment, and allows non-invasive examination of Fe localization. Interestingly, Fe was visualized in tissues outside the endodermis with both Perls-DAB staining and μXRF. The endodermis cells are wrapped into a layer of suberin and sometimes lignin called the Casparian strip. This chemically modified wall controls the permeability of water and ions towards the central cylinder. In *Paspalum urvillei* the casparian strip seems to act as an efficient barrier to Fe since Fe depositions were almost inexistent in the central cylinder (Fig. 4B) and the major part of Fe was found in IP.

Fe K-edge μXANES spectra were collected from μXRF maps on a number of small areas of IP containing various amounts of Fe, some of which are indicated in the map shown in Fig. 4B. Those spectra were compared to Fe reference spectra (Fig. 5). Iron Plaque spectra exhibited a lower K-edge in comparison to Fe(III) compounds, albeit higher than Fe(II) compounds, indicating that Fe in IP is present as a mix of oxidized and reduced forms. Examination of the pre-edge structure confirmed that both oxidation states were present in IP (Fig. 6) and the pre-edge of the control spectrum (0.1 mM Fe) was slightly shifted to lower energy values than the 7 mM Fe exposed samples, suggesting that the proportion of Fe(II) was higher for low exposure. The fingerprint approach using linear combination fitting showed that in IP formed in roots exposed to7 mM Fe, spectra were modeled by a mixture of ferrihydrite and Fe(II)-citrate ranging from 66 ± 10 to 81 ± 10% ferrihydrite and 19 ± 10 to 38 ± 10% Fe(II)-citrate (Fig. 7). Here Fe(II)-citrate was used as a proxy for a non crystallized form of Fe(II) since the crystallized forms siderite and chromite gave poor spectral agreement due to their well defined structure patterns. We can thus infer that Fe partially occurs as a Fe(II) form, organic or poorly crystallized in IP, in addition to ferrihydrite. In the control Fe condition, as suggested by the examination of the pre-edge, the proportion of ferrihydrite decreased (46 ± 10%) while Fe(II) increased (51 ± 10%).

Iron oxyhydroxides have high specific surface areas and possess $^{-}$OH functional groups, which are capable of reacting with metals and other cations and anions (Kuo, 1986). It is likely that the crystalline Fe hydroxides (ferrihydrite) identified around the roots of *Paspalum urvillei* have similar properties and immobilize and prevent the uptake of other elements. The co-localization of Fe and phosphorus on IP indicated that the plaque was probably composed of iron oxide with phosphorus adsorbed onto the surface. Phosphorus is an element easily found on the IP, since phosphate has a high affinity to ferric hydroxides (e.g. ferrihydrite) (Voegelin et al., 2013; Senn et al., 2015).

The sodium dithionite ($Na_2S_2O_4$)-sodium citrate ($Na_3C_6O_7H_5$)-sodium bicarbonate ($NaHCO_3$) (DCB) mixture solution is a classical extraction reagent for IP on root surface (Lee et al., 2013). Previous results with *Paspalum urvillei* using the extraction with DCB technique showed the presence of Fe, zinc, phosphate, and calcium in the IP (de Araujo et al., 2014). Micro-XRF mapping confirmed the occurrence of Ca and P and also revealed the presence of Mn and Si (Zn was not measured since the mapping energy was below the Zn K-absorption edge).

In leaves of control plants, Fe was hardly visible in tissues and cells, for all species (Fig. 8). Leaves of plants treated with Fe excess displayed high Fe accumulation, localized in different cellular compartments. The highest Fe accumulation, common to all species, corresponded the bundle sheath cells (Fig. 8, arrows). Within these cells, Fe highly accumulated in the central vacuole. Additionally, the C4 species (*Paspalum urvillei*, *Setaria parviflora* and *Setaria viridis*) displayed an intense Fe staining in the chloroplasts of the bundle sheath cells, contrary to rice that is a C3 species. Additionally, the Perls/DAB staining could reveal secondary sites of Fe accumulation in mesophyll cells. The chloroplasts of *Paspalum urvillei* and *Oryza sativa* were strongly stained and contained Fe-rich dots (Fig. 8 arrowheads) that had been previously demonstrated to correspond to ferritin complexes (Roschzttardtz et al., 2013). In both *Setaria* species, Fe was much less visible in mesophyll cells, compared to *Paspalum urvillei* and rice and most of the signal was located in bundle sheath cells. The Fe accumulation in these cells was nevertheless much more pronounced in *Setaria viridis*, compared to *Setaria parviflora*, in good agreement with the strong difference in total Fe accumulation between these two species (Fig. 2). Taken together, these results highlight the role of the bundle sheath cells in the sequestration of Fe in leaves, in response to elevated concentrations of Fe in the growth medium. Within these cells, Fe accumulated in the central vacuole for all species but also in chloroplasts for the C4 species *Paspalum urvillei*, *Setaria parviflora* and *Setaria viridis*. The visualization of iron bound to ferritins, the expected main actor in Fe detoxification, could not be strictly correlated with the overall Fe accumulation in leaves of the four species as shown in Fig. 2, since Fe-ferritin structures were mostly visible in *Paspalum urvillei* (low Fe) and rice (high Fe).

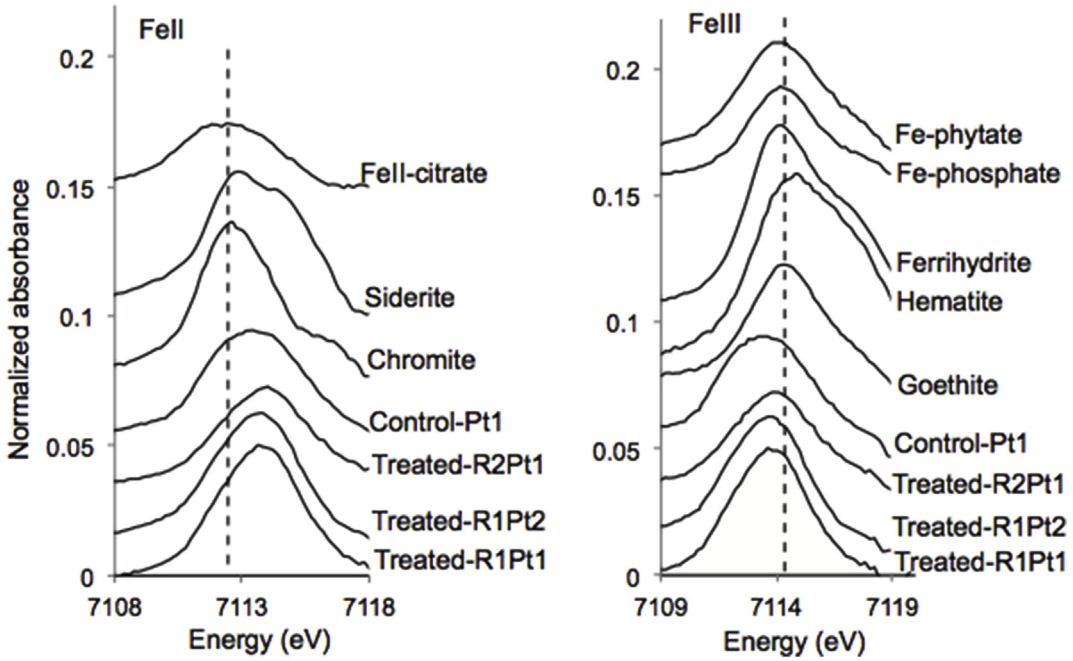

Fig. 6. Normalized pre-edge spectra (Fe K-edge) of *Paspalum urvillei* treated with 0.1 mM (Control) and 7 mM (Treated) Fe-citrate compared to Fe(II) reference spectra (Left) and Fe(III) reference spectra (Right).

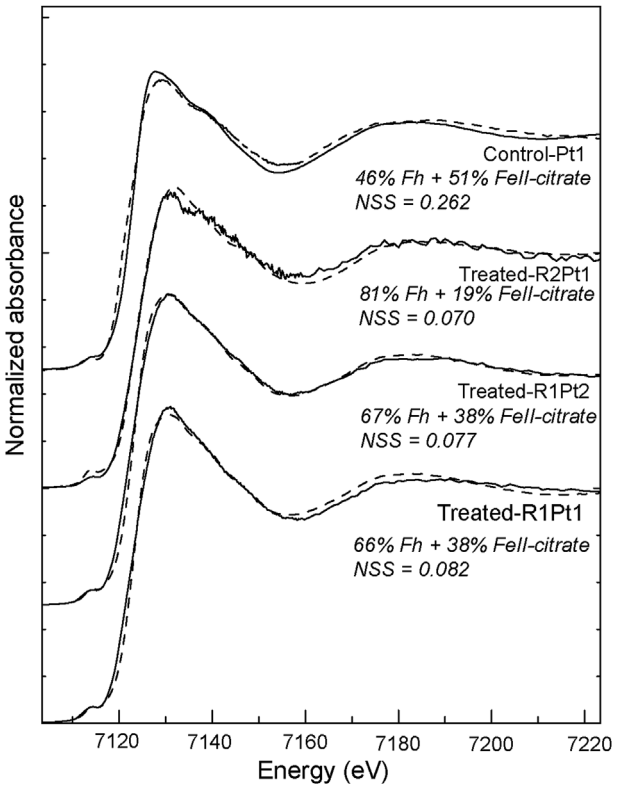

Fig. 7. Linear combination fits of Fe K-edge μXANES spectra for *Paspalum urvillei* treated with 0.1 mM (Control) and 7 mM (Treated) Fe-citrate. The quality of the fit is evaluated by the normalized sum-squares residuals, NSS = $\Sigma i(Xanes_{experimental} - Xanes_{fit})2/\Sigma i(Xanes_{experimental})^2$ x 100.

3.3. Iron speciation in the xylem sap of Setaria parviflora plants

Among the four species considered, only *Setaria parviflora* could yield sufficient amounts of xylem sap to analyze the Fe speciation. The quantification of total Fe in the xylem sap showed that high Fe concentrations in the medium tended to increase the concentration of Fe in the xylem sap (33.15 ppm vs 12.6 ppm) although the high variability of Fe concentration in Fe excess samples prevented to conclude statistically on such effect. Nevertheless, the speciation of Fe in the xylem sap of *Setaria parviflora* plants was analysed by means of hydrophilic interaction chromatography (HILIC) with dual detection: inductively coupled plasma mass spectrometry (ICP-MS) and electrospray ionisation–Fourier-transform mass spectrometry (ESI-FTMS).

The analysis of samples grown in the control condition showed presence of one peak (Fig. 9a) while in the sample grown in Fe excess condition, 2 additional peaks were detected (Fig. 9b) by ICP MS. The ESI MS spectra were searched for the specific isotopic pattern (exact inter-isotopic mass differences and isotopic ratios) at the retention times corresponding to the peaks detected by HPLC ICP MS. The use of the accurate masses of the precursor ions allowed assignment of the empiric molecular formulas to compounds identified as the one containing iron, and their fragmentation led to determination of the structures for all the iron species detected. They were identified as Fe_3Cit_3 for control sample, $Fe_3Cit_2Mal_2$, and $Fe_3Cit_3Mal_1$ in case of plants exposed to Fe excess.

The determination of the concentration of ^{56}FeMalCit complexes in plant samples was performed by adding different amounts of a solution of ^{58}Fe to the plant sample. After addition of ^{58}Fe to the xylem sample, no significant changes were observed in the signal intensity recorded for ^{56}Fe isotope, indicating that there was no exchange between the two Fe isotopes in the samples. Based on calibration curves made with ^{58}Fe, citrate and malate, it was possible to quantify the Fe complexes present in the xylem samples (Table 1). The presence of free ligands (malate and citrate) in samples allowed the formation ^{58}FeMalCit and ^{58}FeCit complexes, what was confirmed by ICP MS (Fig. 10) and ESI MS (Fig. 11). Interestingly, in the control sample, ^{58}Fe was only complexed with citrate (Fig. 9a), compared to the Fe-excess sample, indicating that the xylem of the control sample did not contain sufficient malate to form the FeMalCit complexes that are formed and detected in the Fe-treated sample (Fig. 9b). Therefore, the accumulation of malate and the corresponding formation of FeMalCit appears as a specific response of the plant to the exposure to excess Fe in the medium.

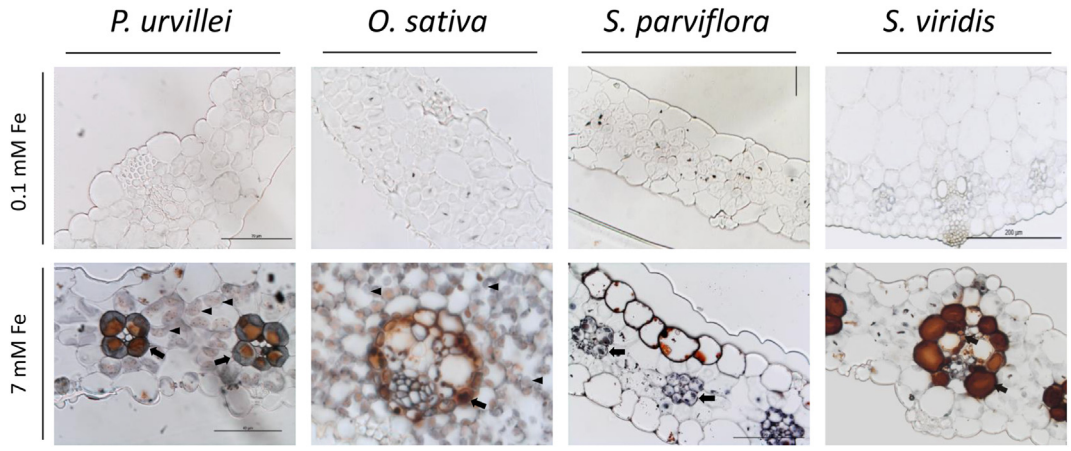

Fig. 8. Fe localization in leaves of *P. urvillei, O. sativa, S. parviflora* and *S. viridis*. Plants were treated with 0.1 mM (A) or 7 mM Fe-Citrate (B–E) during 6 days and shoot samples were further fixed and embedded in resin. Sections were submitted to Perls/DAB staining. Arrows: bundle sheath cells, arrowheads: ferritin-rich chloroplasts.

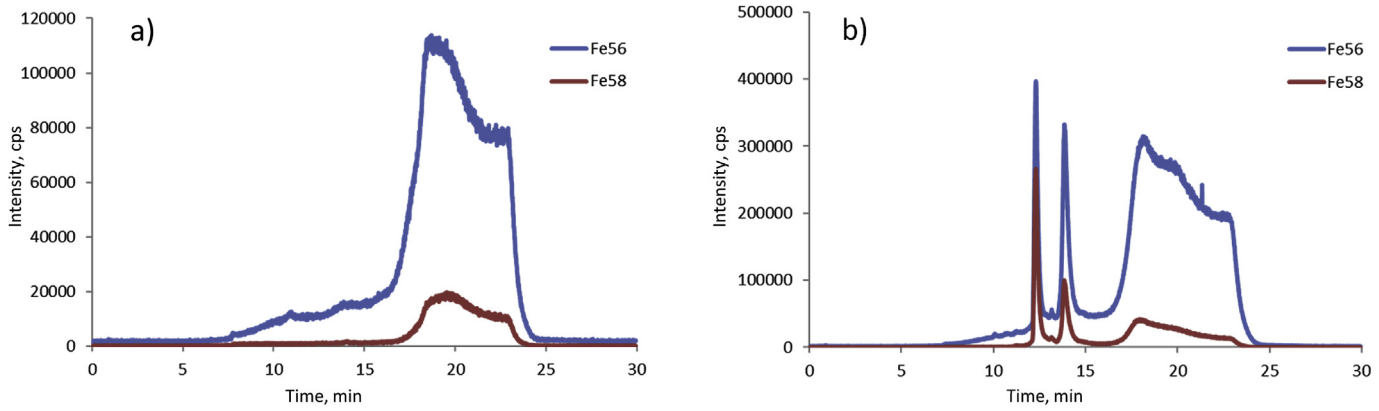

Fig. 9. HILIC ICP MS chromatogram of control (A) and supplemented (B) *S. parviflora* xylem sap samples spiked with ^{58}Fe (column: Phenomenex Kinetex; gradient: 0–1 min 95% B; 1–10 min 85%; 10–15 min 85% B; 15–17 min 65% B; 17–25 min 65% B;25–30 min 95% B, B - ACN and A - 25 mM ammonium acetate in H_2O, pH 5.5; injection: 10 µL; flow rate: 0.5 ml min^{-1}.

Table 1
Quantification of total Fe and Fe complexes identified by HILIC ICP MS in the xylem sap of *Setaria parviflora* plants grow on 0.1 mM and 7 mM Fe-citrate. For the samples annotated "xylem", the corresponding values are the average ± SD of n = 4–5 individual samples. The samples annotated S.p. correspond to individual samples used for the quantification of Fe complexes using the^{58}Fe spiking approach.

	Concentration of 56 Fe in sample [ppm]	Concentration of iron in complex form in sample [ppm]				% of 56 Fe complex in total amount of Fe			
		56Fe3Cit2Mal2	56Fe3Cit3Mal1	56Fe3Cit3	total	56Fe3Cit2Mal2	56Fe3Cit3Mal1	56Fe3Cit3	total
Xylem (0.1 mMFe)	12.6 ± 3								
Xylem (7 mM Fe)	33.15 ± 31.63								
S. p. 0.1 mM	8.6	< LOD	< LOD	< LOD	< LOD	–	–	–	–
S.p. 7 mM	11.0	3.1	3.2	not quantified	6.3	28	29	not quantified	57

4. Discussion

The aim of our work was to investigate the mechanisms of Fe sequestration in plants growing in excess concentrations, using plant species naturally adapted to such conditions. Therefore, our strategy was first to verify that, in laboratory conditions, *Paspalum urvillei* and *Setaria parviflora* were also tolerant to very high Fe concentrations in the medium, by comparing them to either a model grass (rice) or a related species of the same gender (*Setaria viridis*), respectively. Thereafter, we have characterized the responses of young plants to short-term exposure to high Fe in the medium. Although different from the natural environment, our experimental conditions have enabled us to monitor changes in Fe distribution in both roots and shoots, to establish that *Paspalum urvillei* and *Setaria parviflora* were behaving as excluders in condition of Fe excess and to identify the major sites of Fe accumulation at the tissue, cellular and subcellular levels.

In previous reports, *Paspalum urvillei* and *Setaria parviflora* plants treated with high Fe-EDTA concentrations displayed higher Fe content in roots than in shoots and presented symptoms of Fe toxicity (de Araujo et al., 2014; Santana et al., 2014). In this paper, the four plant species were treated with citrate, which is another Fe chelator, with different responses. In addition to high Fe translocation rates towards shoots, *Paspalum urvillei* and *Setaria parviflora* did not show any visual symptoms of toxicity by iron excess, compared to rice and *Setaria viridis*. Actually, it had been previously shown that depending on the culture system and the Fe source, the amount and distribution of apoplastic Fe

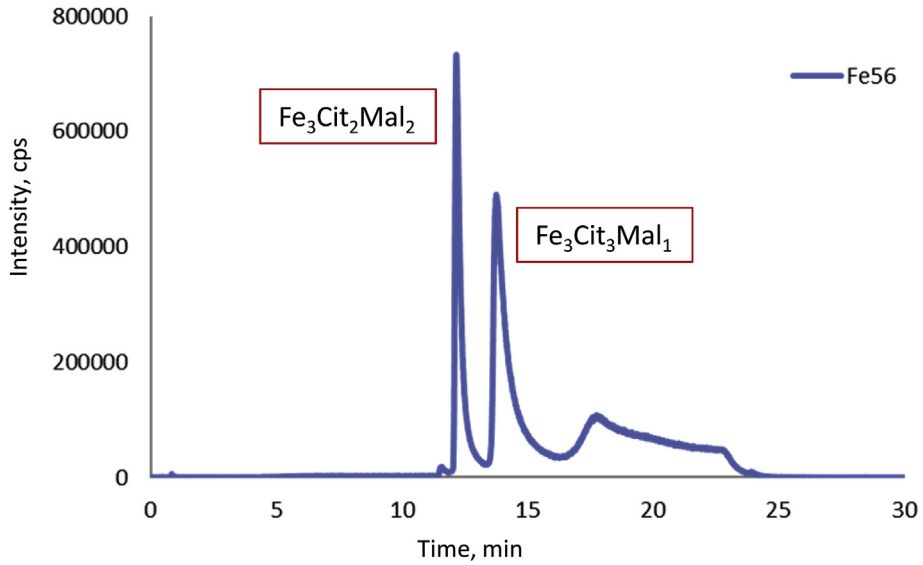

Fig. 10. HILIC - ICP MS chromatogram of the standard citrate-malate iron complexes (chromatographic conditions the same as in Fig. 9).

pool was prone to be overestimated, in particular when using Fe-EDTA (Roschzttardtz et al., 2013; Strasser et al., 1999). The higher toxicity provoked by EDTA-based Fe complexes is most likely due to the high affinity of EDTA towards other metals present in the growth medium (logK = 16.5 for Zn and logK = 18.8 for Cu), with the potential risk of spontaneous formation of the corresponding Zn-EDTA and Cu-EDTA complexes, potentially leading to a "polymetallic" stress. On the contrary, citric acid is rather specific for trivalent metal ions and displays a very poor affinity for divalent metal ions compared to Fe^{3+} (logK = 4.5 for Zn and 6.1 for Cu, compared to 11.85 for Fe^{3+}), which decreases the risk of polymetallic excess stress (http://www.coldcure.com/html/stability_constants.html). Therefore, the data obtained here suggested that the use of Fe-citrate as the source of iron might be a better proxy of the Fe-contaminated soil conditions encountered by *Paspalum urvillei* and *Setaria parviflora*.

The ability of *Paspalum urvillei* and *Setaria parviflora* plants to tolerate high Fe concentrations in the medium is likely to rely on several mechanisms aimed at decreasing the toxicity of this metal, by limiting the uptake at the root surface through the build-up of the iron plaque, limiting the translocation of Fe towards the shoots and by sequestering Fe in the apoplastic compartment, vacuoles, and in plastids as ferritin complexes, away from highly sensitive intracellular sites. Here we evidenced that the IP thickness increased with Fe supply, suggesting that the build-up of IP *via* the precipitation of ferrihydrite was a mechanism of Fe avoidance. Ferrihydrite is an iron mineral phase commonly identified in IP (Hansel et al., 2001, 2002; Liu et al., 2006). The studies of metal speciation in the IP have revealed that actually the composition of the Fe plaque is rather heterogeneous, consisting of a mix of several minerals, including goethite, ferrihydrite, lepidocrocite and siderite, the proportion of each mineral being tightly linked to the local environment of the roots (Snowden and Wheeler, 1995). The origin of the Fe(II) is more questioning since hydroponic cultures were done in oxic conditions where Fe was provided as ferric iron and the nature of this reduced iron could not be clearly identified. Siderite, which was suspected and identified elsewhere and likely formed by CO_2 released by the roots (Hansel et al., 2002; Wang and Peverly, 1996, 1999) was not detected here. In contrast, the Fe phase appeared to be poorly crystallized or organic. Since *Paspalum urvillei* belongs to the grass family, Fe uptake should be achieved via Fe(III)-phytosiderophore and not by iron reduction. It is not excluded here that the root itself is able to reduce part of iron as already proposed by Wang et al. (1999) (Wang and Peverly, 1999). Associated microorganisms including ferric reducing bacteria could also be involved in the Fe redox reaction at the root surface (King and Garey, 1999; Chang et al., 2014; Tian et al., 2015). The Fe(II) proportion was higher in control than in Fe excess conditions, suggesting that Fe reduction was not related to the amount of Fe in solution but rather to a limited biological process.

Since the pioneering work of Bienfait et al. (1985) on the biochemical characterization of the cell wall binding capacity towards Fe, this compartment has received little attention in the context of Fe homeostasis. Only recently, several reports have uncovered dynamic responses of cell wall components in response to Fe deficiency, including decrease in hemicellulose concentration and methylation to lower the retention of apoplastic Fe and promote its remobilization (Lei et al., 2014; Ye et al., 2015; Curie and Mari, 2017). Nevertheless, the role of the cell wall as a buffering compartment in conditions of Fe overload has been much less characterized. Here, thanks to the Perls/DAB staining procedure, it has been possible to highlight the role of the cell wall as a buffer for Fe excess in the root epidermal and cortical cells (Fig. 2). Although the chemical form of this apoplastic Fe pool remains unknown, in the Fe hyperaccumulator plant species *Imperata cylindrica*, cell wall Fe deposits were shown to correspond to jarosite, an iron and sulfur-rich mineral (Rodriguez et al., 2005; Amils et al., 2007). Although it is tempting to propose that, as for *Imperata cylindrica*, in cell walls of *Paspalum urvillei* and *Setaria parviflora* Fe is biomineralized as jarosite, this is very unlikely since jarosite crystals are formed only in sulfur-rich and highly acidic conditions, which was not the case for *Paspalum urvillei* or *Setaria parviflora*. The chemical identity of this Fe pool remains thus unknown but this finding also raises the question of the specific properties and modifications of the root apoplastic compartment of this particular Fe tolerant species, as a response to Fe overload, by comparison with the biochemical responses of the cell wall components in Fe deficiency.

Ferritin expression can be considered as the hallmark of molecular responses to Fe excess (Briat et al., 1995a, 1995b, 2010b). Ferritins accumulate in plastids in response to Fe excess, where they assemble in 24-mer structures that can bind up to 4500 Fe atoms. However, despite the high Fe-buffering capacity of ferritins, the exact role of these proteins in iron detoxification mechanisms remains elusive since ferritin-null mutants in the model plant *Arabidopsis thaliana* are only slightly affected by Fe excess (Ravet et al., 2008). In a previous report, we had shown that iron-ferritin complexes could be efficiently visualized by histochemical staining with the Perls/DAB procedure, as individual dots in plastids (Roschzttardtz et al., 2013; Ravet et al., 2008). Here, beside the bundle sheath cells where Fe highly accumulated in vacuoles, iron-ferritin structures could readily be detected in mesophyll

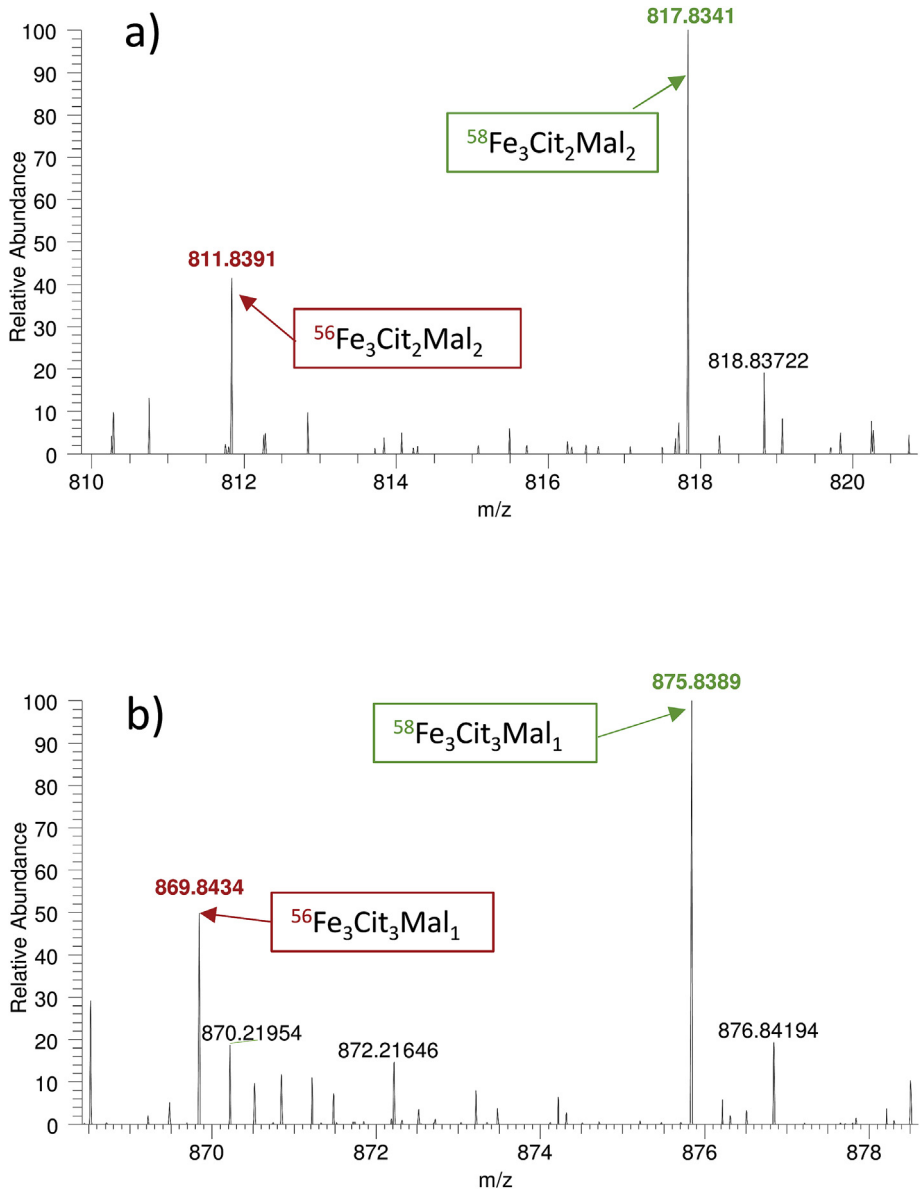

Fig. 11. ESI MS spectra taken at the peak apexes at RT 12.23 min (A) and at RT 14.21 min (B) showing isotopic patterns of $Fe_3Cit_2Mal_2$ and Fe_3Cit_3Mal species respectively; mono-isotopic mass in red, mass corresponding to added isotope ^{58}Fe marked in green. (For interpretation of the references to color in this figure legend, the reader is referred to the Web version of this article.)

cells, where they could represent an important part of Fe-rich detectable compounds accumulated (Fig. 8). Therefore, in photosynthetic tissues, ferritins seem to play an important role in buffering the excess of Fe that had been translocated from roots to leaves. However, on the basis of the intensity of the Fe staining in chloroplasts, it was not possible to correlate the total amount of Fe in shoots (Fig. 2) with the imaging of Fe (Fig. 8). It is thus difficult to use this information directly as a proxy of Fe accumulation and detoxification capacity in leaves.

In roots and bundle sheath cells of *Paspalum urvillei, Oryza sativa and Setaria parviflora*, iron was massively accumulated in vacuoles. Although vacuolar storage appears as an obvious way to sequester Fe, only in few instances this mechanism has been clearly described. To date, the best example is represented by the Arabidopsis embryo, where Fe was shown to accumulate in vacuoles of a specific cell layer, the endodermis, in globoids that are phytate-rich structures (Roschzttardtz et al., 2009; Ravet et al., 2008; Lanquar et al., 2005; Kim et al., 2006). The transport of Fe in these vacuoles is mediated by the tonoplastic iron transporter VIT1 (Ravet et al., 2008; Kim et al., 2006), whereas the efflux from vacuoles that occurs during germination to remobilize the Fe atoms is catalyzed by NRAMP3 and NRAMP4 (Lanquar et al., 2005). It is therefore tempting to propose that in *Paspalum urvillei, Setaria parviflora* and rice, VIT1 orthologs might be overexpressed in response to Fe excess, to mediate vacuolar sequestration of Fe through transport across the tonoplast. Although the chemical form of Fe that is stored in vacuoles remains uncharacterized, the granular aspect of Perls/DAB-stained Fe in *Paspalum urvillei, Oryza sativa* and *Setaria parviflora* vacuoles was quite comparable to the vacuolar Fe oxides observed by electron microscopy in the Fe hyperaccumulator *Imperata cylindrica* (Fuente et al., 2016; Raymond et al., 2003) and in maize seedlings exposed to Fe_2O_3 nanoparticles (Li et al., 2016). Taken together, these elements of comparison tend to suggest that upon Fe overload, the strategy developed by those species would be to accumulate most of the Fe in vacuoles as ferric iron oxides.

5. Conclusion

We have shown that *Paspalum urvillei* and *Setaria parviflora* can tolerate high Fe concentrations in the medium through selected exclusion and detoxification (vacuole, cell wall) mechanisms leading to an excluder behavior, when compared with less tolerant species. Iron exclusion is achieved by the build up of a barrier, the iron plaque, where Fe is immobilized as ferrihydrite. The intracellular detoxification response appears to rely mostly on the sequestration of Fe into cell walls and vacuoles. In leaves, the vacuole would represent the main intracellular site of ferric oxide buildup, strongly suggesting the high importance of vacuolar sequestration in the detoxification of excess Fe in these species.

Declaration of competing interest

The authors declare that they have no known competing financial interests or personal relationships that could have appeared to influence the work reported in this paper.

Acknowledgments

This study was financed in part by the Coordenação de Aperfeiçoamento de Pessoal de Nível Superior - Brasil (CAPES) – Finance Code 001 for the doctoral fellowship of T.O. Araújo and to CNPq (National Council for Scientific and Technological Development, Brazil) for providing research scholarship to L.C. Silva (309308/2018-6). We also thank the Soleil Synchrotron (Gif sur Yvette, France) for the provision of beamtime on the LUCIA beamline and the French National Research Agency for the funding (projet ANR-12-BSV2-0020-01, “SUBCELIF” and EQUIPEX-MARSS ANR-11-EQPX-0027).

References

Amils, R., de la Fuente, V., Rodriguez, N., Zuluaga, J., Menendez, N., Tornero, J., 2007. Composition, speciation and distribution of iron minerals in Imperata cylindrica. Plant Physiol. Biochem. 45, 335–340.

Bacha, R.E., Hossner, L.R., 1977. Characteristics of coatings formed on rice roots as affected by iron and manganese additions. Soil Sci. Soc. Am. J. 41, 931–935.

Balk, J., Schaedler, T.A., 2014. Iron cofactor Assembly in plants. Annu. Rev. Plant Biol. 65, 65 125-+.

Batty, L.C., Baker, A.J.M., Wheeler, B.D., Curtis, C.D., 2000. The effect of pH and plaque on the uptake of Cu and Mn in Phragmites australis (Cav.) Trin ex. Steudel. Ann. Bot. 86, 647–653.

Bienfait, H.F., Briel, W.v.d., Mesland-Mul, N.T., 1985. Free space iron pools in roots. Generation and mobilization. Plant Physiol. 78, 596–600.

Blute, N.K., Brabander, D.J., Hemond, H.F., Sutton, S.R., Newville, M.G., Rivers, M.L., 2004. Arsenic sequestration by ferric iron plaque on cattail roots. Environ. Sci. Technol. 38, 6074–6077.

Bothe, H., Slomka, A., 2017. Divergent biology of facultative heavy metal plants. J. Plant Physiol. 219, 45–61.

Bournier, M., Tissot, N., Mari, S., Boucherez, J., Lacombe, E., Briat, J.F., Gaymard, F., 2013. Arabidopsis ferritin 1 (AtFer1) gene regulation by the phosphate starvation response 1 (AtPHR1) transcription factor reveals a direct molecular link between iron and phosphate homeostasis. J. Biol. Chem. 288, 22670–22680.

Briat, J.F., Fobis-Loisy, I., Grignon, N., Lobréaux, S., Pascal, N., Savino, G., Thoiron, S., von Wiren, N., Van Wuytswinkel, O., 1995a. Cellular and molecular aspects of iron metabolism in plants. Biol. Cell. 84, 69–81.

Briat, J.F., Labouré, A.M., Laulhère, A.P., Lescure, A.M., Lobréaux, S., Pesay, H., Proudhon, D., Wuitswinkel, O., 1995b. In: Abadia, J. (Ed.), Molecular and Cellular Biology of Plant Ferritins, Iron Nutrition in Soils and Plants, pp. 265–276.

Briat, J.F., Ravet, K., Arnaud, N., Duc, C., Boucherez, J., Touraine, B., Cellier, F., Gaymard, F., 2010a. New insights into ferritin synthesis and function highlight a link between iron homeostasis and oxidative stress in plants. Ann. Bot. 105, 811–822.

Briat, J.F., Duc, C., Ravet, K., Gaymard, F., 2010b. Ferritins and iron storage in plants. Biochim. Biophys. Acta Gen. Subj. 1800, 806–814.

Chang, H.S., Buettner, S.W., Seaman, J.C., Jaffé, P.R., Koster Van Groos, P.G., Li, D., Peacock, A.D., Scheckel, K.G., Kaplan, D.I., 2014. Uranium immobilization in an iron-rich rhizosphere of a native wetland plant from the savannah river site under reducing conditions. Environ. Sci. Technol. 48, 9270–9278.

Chen, C.C., Dixon, J.B., Turner, F.T., 1980. Iron coatings on rice roots - morphology and models of development. Soil Sci. Soc. Am. J. 44, 1113–1119.

Curie, C., Mari, S., 2017. New routes for plant iron mining. New Phytol. 214, 521–525.

de Araujo, T.O., de Freitas-Silva, L., Santana, B.V.N., Kuki, K.N., Pereira, E.G., Azevedo, A.A., da Silva, L.C., 2014. Tolerance to iron accumulation and its effects on mineral composition and growth of two grass species. Environ. Sci. Pollut. Res. 21, 2777–2784.

de Araujo, T.O., de Freitas-Silva, L., Santana, B.V.N., Kuki, K.N., Pereira, E.G., Azevedo, A.A., da Silva, L.C., 2015. Morphoanatomical responses induced by excess iron in roots of two tolerant grass species. Environ. Sci. Pollut. Res. 22, 2187–2195.

de la Fuente, V., Rufo, L., Rodríguez, N., Franco, A., Amils, R., 2017. Comparison of iron localization in wild plants and hydroponic cultures of Imperata cylindrica (L.) P. Beauv. Plant Soil 418, 25–35.

Dinakar, C., Abhaypratap, V., Yearla, S.R., Raghavendra, A.S., Padmasree, K., 2010. Importance of ROS and antioxidant system during the beneficial interactions of mitochondrial metabolism with photosynthetic carbon assimilation. Planta 231, 461–474.

Feng, H., Zhang, W., Liu, W., Yu, L., Qian, Y., Wang, J., Wang, J.J., Eng, C., Liu, C.J., Jones, K.W., Tappero, R., 2015. Synchrotron micro-scale study of trace metal transport and distribution in Spartina alterniflora root system in Yangtze River intertidal zone. Environ. Sci. Pollut. Res. 22, 18933–18944.

Fuente, V., Rufo, L., Juarez, B.H., Menendez, N., Garcia-Hernandez, M., Salas-Colera, E., Espinosa, A., 2016. Formation of biomineral iron oxides compounds in a Fe hyperaccumulator plant: Imperata cylindrica (L.) P. Beauv,. J. Struct. Biol. 193, 23–32.

Green, M.S., Etherington, J.R., 1977. Oxidation of ferrous iron by rice (Oryza-Sativa-L) roots - mechanism for waterlogging tolerance. J. Exp. Bot. 28, 678–&.

Grillet, L., Ouerdane, L., Flis, P., Hoang, M.T.T., Isaure, M.-P., Lobinski, R., Curie, C., Mari, S., 2014. Ascorbate efflux as a new strategy for iron reduction and transport in plants. J. Biol. Chem. 289, 2515–2525.

Hansel, C.M., Fendorf, S., Sutton, S., Newville, M., 2001. Characterization of Fe plaque and associated metals on the roots of mine-waste impacted aquatic plants. Environ. Sci. Technol. 35, 3863–3868.

Hansel, C.M., La Force, M.J., Fendorf, S., Sutton, S., 2002. Spatial and temporal association of as and Fe species on aquatic plant roots. Environ. Sci. Technol. 36, 1988–1994.

Hu, Z.Y., Zhu, Y.G., Li, M., Zhang, L.G., Cao, Z.H., Smith, E.A., 2007. Sulfur (S)-induced enhancement of iron plaque formation in the rhizosphere reduces arsenic accumulation in rice (Oryza sativa L.) seedlings. Environ. Pollut. 147, 387–393.

Huang, Y.C., Chen, Z., Liu, W.J., 2012. Influence of iron plaque and cultivars on antimony uptake by and translocation in rice (Oryza sativa L.) seedlings exposed to Sb(III) or Sb (V). Plant Soil 352, 41–49.

Isaure, M.-P., Huguet, S., Meyer, C.-L., Castillo-Michel, H., Testemale, D., Vantelon, D., Saumitou-Laprade, P., Verbruggen, N., Sarret, G., 2015. Evidence of various mechanisms of Cd sequestration in the hyperaccumulator Arabidopsis halleri, the non-accumulator Arabidopsis lyrata, and their progenies by combined synchrotron-based techniques. J. Exp. Bot. 66, 3201–3214.

Kim, S.A., Punshon, T., Lanzirotti, A., Li, L., Alonso, J.M., Ecker, J.R., Kaplan, J., Guerinot, M.L., 2006. Localization of iron in Arabidopsis seed requires the vacuolar membrane transporter VIT1. Science 314, 1295–1298.

King, G.M., Garey, M.A., 1999. Ferric iron reduction by bacteria associated with the roots of freshwater and marine macrophytes. Appl. Environ. Microbiol. 65, 4393–4398.

Kobayashi, T., Nishizawa, N.K., 2012. Iron uptake, translocation, and regulation in higher plants. In: In: Merchant, S.S. (Ed.), Annual Review of Plant Biology, vol 63. Annual Reviews, Palo Alto, pp. 131–152.

Kuo, S., 1986. Concurrent sorption of phosphate and zinc, cadmium, or calcium by A hydrous ferric-oxide. Soil Sci. Soc. Am. J. 50, 1412–1419.

Lanquar, V., Lelievre, F., Bolte, S., Hames, C., Alcon, C., Neumann, D., Vansuyt, G., Curie, C., Schroder, A., Kramer, U., Barbier-Brygoo, H., Thomine, S., 2005. Mobilization of vacuolar iron by AtNRAMP3 and AtNRAMP4 is essential for seed germination on low iron. EMBO J. 24, 4041–4051.

Lee, C.H., Hsieh, Y.C., Lin, T.H., Lee, D.Y., 2013. Iron plaque formation and its effect on arsenic uptake by different genotypes of paddy rice. Plant Soil 363, 231–241.

Lei, G.J., Zhu, X.F., Wang, Z.W., Dong, F., Dong, N.Y., Zheng, S.J., 2014. Abscisic acid alleviates iron deficiency by promoting root iron reutilization and transport from root to shoot in Arabidopsis. Plant Cell Environ. 37, 852–863.

Li, J.L., Hu, J., Ma, C.X., Wang, Y.Q., Wu, C., Huang, J., Xing, B.S., 2016. Uptake, translocation and physiological effects of magnetic iron oxide (gamma-Fe2O3) nanoparticles in corn (Zea mays L.). Chemosphere 159, 326–334.

Liu, W.J., Zhu, Y.G., Hu, Y., Williams, P.N., Gault, A.G., Meharg, A.A., Charnock, J.M., Smith, F.A., 2006. Arsenic sequestration in iron plaque, its accumulation and speciation in mature rice plants (Oryza Sativa L.). Environ. Sci. Technol. 40, 5730–5736.

Liu, J.G., Leng, X.M., Wang, M.X., Zhu, Z.Q., Dai, Q.H., 2011. Iron plaque formation on roots of different rice cultivars and the relation with lead uptake. Ecotoxicol. Environ. Saf. 74, 1304–1309.

Muller, C., Kuki, K.N., Pinheiro, D.T., de Souza, L.R., Silva, A.I.S., Loureiro, M.E., Oliva, M.A., Almeida, A.M., 2015. Differential physiological responses in rice upon exposure to excess distinct iron forms. Plant Soil 391, 123–138.

Nozoye, T., Nagasaka, S., Kobayashi, T., Takahashi, M., Sato, Y., Uozumi, N., Nakanishi, H., Nishizawa, N.K., 2011. Phytosiderophore efflux transporters are crucial for iron acquisition in graminaceous plants. J. Biol. Chem. 286, 5446–5454.

Pardo, T., Martínez-Fernández, D., de la Fuente, C., Clemente, R., Komárek, M., Bernal, M.P., 2016. Maghemite nanoparticles and ferrous sulfate for the stimulation of iron plaque formation and arsenic immobilization in Phragmites australis. Environ. Pollut. 219, 296–304.

Pereira, E.G., Oliva, M.A., Siqueira-Silva, A.I., Rosado-Souza, L., Pinheiro, D.T., Almeida, A.M., 2014. Tropical rice cultivars from lowland and upland cropping systems differ in iron plaque formation. J. Plant Nutr. 37, 1373–1394.

Pi, N., Tam, N.F.Y., Wong, M.H., 2011. Formation of iron plaque on mangrove roots receiving wastewater and its role in immobilization of wastewater-borne pollutants. Mar. Pollut. Bull. 63, 402–411.

Ravet, K., Touraine, B., Boucherez, J., Briat, J.F., Gaymard, F., Cellier, F., 2008. Ferritins

control interaction between iron homeostasis and oxidative stress in Arabidopsis. Plant J. 57, 400–412.
Raymond, K.N., Dertz, E.A., Kim, S.S., 2003. Enterobactin: an archetype for microbial iron transport. Proc. Natl. Acad. Sci. U. S. A. 100, 3584–3588.
Reeves, R.D., Baker, A.J.M., Jaffré, T., Erskine, P.D., Echevarria, G., van der Ent, A., 2018. A global database for plants that hyperaccumulate metal and metalloid trace elements. New Phytol. 218, 407–411.
Rellan-Alvarez, R., Giner-Martinez-Sierra, J., Orduna, J., Orera, I., Rodriguez-Castrillon, J.A., Garcia-Alonso, J.I., Abadia, J., Alvarez-Fernandez, A., 2010. Identification of a tri-iron(III), tri-citrate complex in the xylem sap of iron-deficient tomato resupplied with iron: new insights into plant iron long-distance transport. Plant Cell Physiol. 51, 91–102.
Rodriguez, N., Menendez, N., Tornero, J., Amils, R., de la Fuente, V., 2005. Internal iron biomineralization in Imperata cylindrica, a perennial grass: chemical composition, speciation and plant localization. New Phytol. 165, 781–789.
Roschzttardtz, H., Conejero, G., Curie, C., Mari, S., 2009. Identification of the endodermal vacuole as the iron storage compartment in the Arabidopsis embryo. Plant Physiol. 151, 1329–1338.
Roschzttardtz, H., Conejero, G., Divol, F., Alcon, C., Verdeil, J.-L., Curie, C., Mari, S., 2013. New insights into Fe localization in plant tissues. Front. Plant Sci. 4, 11.
Salt, D.E., Prince, R.C., Pickering, I.J., 2002. Chemical speciation of accumulated metals in plants: evidence from X-ray absorption spectroscopy. Microchem. J. 71, 255–259.
Santana, B.V.N., de Araujo, T.O., Andrade, G.C., de Freitas-Silva, L., Kuki, K.N., Pereira, E.G., Azevedo, A.A., da Silva, L.C., 2014. Leaf morphoanatomy of species tolerant to excess iron and evaluation of their phytoextraction potential. Environ. Sci. Pollut. Res. 21, 2550–2562.
Sarret, G., Smits, E., Michel, H.C., Isaure, M.P., Zhao, F.J., Tappero, R., 2013. Use of synchrotron-based techniques to elucidate metal uptake and metabolism in plants. In: In: Sparks, D.L. (Ed.), Advances in Agronomy, vol 119. Elsevier Academic Press Inc, San Diego, pp. 1–+.
Senn, A.C., Kaegi, R., Hug, S.J., Hering, J.G., Mangold, S., Voegelin, A., 2015. Composition and structure of Fe(III)-precipitates formed by Fe(II) oxidation in water at near-neutral pH: interdependent effects of phosphate, silicate and Ca. Geochem. Cosmochim. Acta 162, 220–246.
Snowden, R.E.D., Wheeler, B.D., 1995. Chemical changes in selected wetland plant species with increasing Fe supply, with specific reference to root precipitates and Fe tolerance. New Phytol. 131, 503–520.
Stcyr, L., Fortin, D., Campbell, P.G.C., 1993. Microscopic observations of the iron plaque of A submerged aquatic plant (Vallisneria-Americana michx). Aquat. Bot. 46, 155–167.
Stein, R.J., Lopes, S.I.G., Fett, J.P., 2014. Iron toxicity in field-cultivated rice: contrasting tolerance mechanisms in distinct cultivars. Theor. Exp. Plant Physiol. 26, 135–146.
Strasser, O., Kohl, K., Romheld, V., 1999. Overestimation of apoplastic Fe in roots of soil grown plants. Plant Soil 210, 179–187.
Takahashi, M., Terada, Y., Nakai, I., Nakanishi, H., Yoshimura, E., Mori, S., Nishizawa, N.K., 2003. Role of nicotianamine in the intracellular delivery of metals and plant reproductive development. Plant Cell 15, 1263–1280.
Taylor, G.J., Crowder, A.A., 1983. Use of the dcb technique for extraction of hydrous iron-oxides from roots of wetland plants. Am. J. Bot. 70, 1254–1257.
Taylor, G.J., Crowder, A.A., Rodden, R., 1984. Formation and morphology of an iron plaque on the roots of typha-latifolia L grown in solution culture. Am. J. Bot. 71, 666–675.
Tian, C., Wang, C., Tian, Y., Wu, X., Xiao, B., 2015. Effects of root radial oxygen loss on microbial communities involved in Fe redox cycling in wetland plant rhizosphere sediment. Fresenius Environ. Bull. 24, 3956–3962.
Tripathi, R.D., Tripathi, P., Dwivedi, S., Kumar, A., Mishra, A., Chauhan, P.S., Norton, G.J., Nautiyal, C.S., 2014. Roles for root iron plaque in sequestration and uptake of heavy metals and metalloids in aquatic and wetland plants. Metall 6, 1789–1800.
van der Ent, A., Baker, A.J.M., Reeves, R.D., Pollard, A.J., Schat, H., 2013. Hyperaccumulators of metal and metalloid trace elements: facts and fiction. Plant Soil 362, 319–334.
Vantelon, D., Trcera, N., Roy, D., Moreno, T., Mailly, D., Guilet, S., Metchalkov, E., Delmotte, F., Lassalle, B., Lagarde, P., Flank, A.M., 2016. The LUCIA beamline at SOLEIL. J. Synchrotron Radiat. 23, 635–640.
Voegelin, A., Senn, A.C., Kaegi, R., Hug, S.J., Mangold, S., 2013. Dynamic Fe-precipitate formation induced by Fe(II) oxidation in aerated phosphate-containing water. Geochem. Cosmochim. Acta 117, 216–231.
Wang, T., Peverly, J.H., 1996. Oxidation states and fractionation of plaque iron on roots of common reeds. Soil Sci. Soc. Am. J. 60, 323–329.
Wang, T., Peverly, J.H., 1999. Iron oxidation states on root surfaces of a wetland plant (Phragmites australis). Soil Sci. Soc. Am. J. 63, 247–252.
Williams, P.N., Santner, J., Larsen, M., Lehto, N.J., Oburger, E., Wenzel, W., Glud, R.N., Davison, W., Zhang, H., 2014. Localized flux maxima of arsenic, lead, and iron around root apices in flooded lowland rice. Environ. Sci. Technol. 48, 8498–8506.
Xu, D.F., Xu, J.M., He, Y., Huang, P.M., 2009. Effect of iron plaque formation on phosphorus accumulation and availability in the rhizosphere of wetland plants. Water Air Soil Pollut. 200, 79–87.
Xu, Y., Sun, X., Zhang, Q., Li, X., Yan, Z., 2018. Iron plaque formation and heavy metal uptake in Spartina alterniflora at different tidal levels and waterlogging conditions. Ecotoxicol. Environ. Saf. 153, 91–100.
Ye, Y.Q., Jin, C.W., Fan, S.K., Mao, Q.Q., Sun, C.L., Yu, Y., Lin, X.Y., 2015. Elevation of NO production increases Fe immobilization in the Fe-deficiency roots apoplast by decreasing pectin methylation of cell wall. Sci. Rep. 5, 13.
Zhang, Y., Xu, Y.H., Yi, H.Y., Gong, J.M., 2012. Vacuolar membrane transporters OsVIT1 and OsVIT2 modulate iron translocation between flag leaves and seeds in rice. Plant J. 72, 400–410.